Influence of Microstucture on the Charge Storage Properties of Chemically Synthesized Manganese Dioxide

Mathieu Toupin,[†] Thierry Brousse,[†,‡] and Daniel Bélanger*[,†]

Laboratoire d'Electrochimie Appliquée, Département de Chimie, Université du Québec à Montréal, Case Postale 888, succursale Centre-Ville, Montréal, Québec H3C 3P8, Canada, and Laboratoire de Génie des Matériaux, Ecole Polytechnique de l'Université de Nantes, La Chantrerie, rue Christian Pauc, BP 50609, 44306 Nantes Cedex 3, France

Received April 23, 2002. Revised Manuscript Received July 2, 2002

α-MnO_2 was synthesized by a very simple coprecipitation technique and tested as active electrode material for an electrochemical supercapacitor. The powder presents a poorly crystallized cryptomelane phase with a chemical composition of $K_{0.05}MnO_2H_{0.10}\cdot 0.15H_2O$. Different aqueous electrolytes were tested including 0.1 M Na_2SO_4, 0.5 M K_2HPO_4/KH_2PO_4 buffer solution, 0.3 M H_2SO_4, and 1 M NaOH, but interesting pseudocapacitance behavior was only observed in the case of 0.1 M Na_2SO_4. Further testing using this electrolyte showed that an average capacitance of 166 F/g can be reproducibly obtained within a voltage range −0.4/+0.5 V vs Hg/Hg_2SO_4 using a sweep rate of 2 mV/s. This interesting value is mainly due to the chimisorption of Na^+ ions and/or protons at the surface of the α-MnO_2 electrode. Nearly all the Mn surface atoms are involved in the pseudocapacitive process. Therefore, the high specific capacitance seems to be related to the high surface area of the MnO_2 powder rather than intercalation of Na^+ ions and/or protons in the structure of α-MnO_2. An optimum composition of 80% of active material in the composite electrode was determined. With such a composition, the α-MnO_2 electrode can withstand 1000 cycles with 100% capacitance retention.

Introduction

Supercapacitors are currently extensively studied as possible auxiliary energy storage devices to be used with rechargeable batteries. They combine the advantages of both dielectric capacitors, which can deliver high power within a very small period, and rechargeable batteries, which store high energy.[1] Electrochemical supercapacitors can be divided into three main categories: (i) carbon/carbon,[2,3] (ii) metal oxides,[4,5] and (iii) electronically conducting polymers.[6,7] The last two kinds of systems involve pseudo-faradaic reactions unlike carbon systems, which use the double-layer capacitance arising from the separation of charge at the interface between the solid electrode and an electrolyte.

Amorphous hydrated RuO_2 exhibits high specific capacitance (720 F/g) within a 1.4-V potential window.[4,8] This is mainly due to redox processes occurring not only at the surface but also inside the bulk of the material. Despite interesting capacitance values, RuO_2 is an expensive material; it is toxic and requires the use of a strong acidic electrolyte (5 M H_2SO_4), which will probably limit its use in electrochemical supercapacitors.

Other metal oxides have also been tested as possible candidates for electrochemical supercapacitor devices. Interesting capacitance values have been reported for IrO_2[9] or CoO_x [10]electrodes but they are still expensive compounds working in strong acidic or alkaline media. On the other hand, MoO_3,[11] molybdenum nitride,[12] nickel oxides,[5] V_2O_5,[13] and MnO_2[14−18] systems seem more promising due to their lower cost. In this latter

* To whom correspondence should be addressed. E-mail: belanger.daniel@uqam.ca.
† Université du Québec à Montréal.
‡ Ecole Polytechnique de l'Université de Nantes.

(1) Conway, B. E. *Electrochemical Supercapacitors, Scientific Fundamentals and Technological Applications*; Kluwer Academic/Plenum Press: New York, 1999.
(2) Morimoto, T.; Hiratsuka, K.; Sanada, Y.; Kurihara, K. *J. Power Sources* **1996**, *60*, 239.
(3) Gamby, J.; Taberna, P. L.; Simon, P.; Fauvarque, J. F.; Chesneau, M. *J. Power Sources* **2001**, *101*, 109.
(4) Zheng, J. P.; Cygan, P. J.; Jow, T. R. *J. Electrochem. Soc.* **1995**, *142*, 2699.
(5) Liu, K. C.; Anderson, M. A. *J. Electrochem. Soc.* **1996**, *143*, 124.
(6) Novak, P.; Müller, K.; Santanam, K. S. V.; Hass, O. *Chem. Rev.* **1997**, *97*, 207.
(7) Soudan, P.; Lucas, P.; Ho, H. A.; Jobin, D.; Breau, L.; Bélanger, D. *J. Mater. Chem.* **2001**, *11*, 773.
(8) Yoon, Y. S.; Cho, W. I.; Lim, J. H.; Choi, D. J. *J. Power Sources* **2001**, *101*, 126.
(9) Conway, B. E.; Birss, V.; Wojtowicz, J. *J. Power Sources* **1997**, *66*, 1.
(10) Lin, C.; Ritter, J. A.; Popov, B. N. *J. Electrochem. Soc.* **1998**, *145*, 4097.
(11) Sugimoto, W.; Ohnuma, T.; Murakami, Y.; Takasu, Y. *Electrochem. Solid-State Lett.* **2001**, *4*, A145.
(12) Liu, T. C.; Pell, W. G.; Conway, B. E.; Roberson, S. L. *J. Electrochem. Soc.* **1998**, *145*, 1882.
(13) Lee, H. Y.; Goodenough, J. B. *J. Solid State Chem.* **1999**, *148*, 81.
(14) Lee, H. Y.; Goodenough, J. B. *J. Solid State Chem.* **1999**, *144*, 220.
(15) Pang, S. C.; Anderson, M. A.; Chapman, T. W. *J. Electrochem. Soc.*, **2000**, *147*, 444.
(16) Lee, H. Y.; Kim, S. W.; Lee, H. Y. *Electrochem. Solid-State Lett.* **2001**, *4*, A19.
(17) Hu, C. C.; Tsou, T. W. *Electrochem. Comm.* **2002**, *4*, 105.
(18) Chin, S. F.; Pang, S. C.; Anderson, M. A. *J. Electrochem. Soc.* **2002**, *149*, A379.

10.1021/cm020408q CCC: $22.00
Published on Web 08/13/2002

case, a huge amount of work has already been performed with MnO_2 compounds in battery applications,[19,20] but up to now only few papers dealt with its use in electrochemical supercapacitors.[14−18] Additionally, the large variety of MnO_2 compounds that can be found as minerals[21] or synthesized via various methods[22] offer a wide range of possibilities for testing this material as a possible candidate for an electrochemical supercapacitor.

In this paper, a MnO_2 compound prepared by a simple coprecipitation technique was studied as a possible active electrode material in an aqueous electrochemical supercapacitor. The aim of this work is to try to identify the factors that control the charge storage characteristic of manganese dioxide and to correlate its electrochemical performance with its structural and microstructural properties.

Experimental Section

Synthesis and Characterization of As-Synthesized Manganese Dioxide. The MnO_2 powder was synthesized using a simple coprecipitation method. $KMnO_4$ (99% purity) was first dissolved in deionized water. While the solution was stirred, $MnSO_4$ was added. The $KMnO_4/MnSO_4$ molar ratio was 2:3. A dark brown precipitate was immediately obtained according to

$$2Mn^{7+} + 3Mn^{2+} \rightarrow 5Mn^{4+} \quad (1)$$

The solution was filtered (Whatman no. 54 paper filter). The precipitate was then dispersed in deionized water and stirred for 5 min using an ultrasonic bath. The same operation was carried out three times. The resulting powder was then dried at 45 °C for 6 h under vacuum. The powder was used as dried or additional thermal treatments were carried out in a tubular oven under N_2 flow. The time and temperature of the annealing treatments will be specified when necessary.

For the quantitative determinations of K and Mn, about 0.1 g of powder was dissolved in 6 M H_2SO_4. Subsequent heating and stirring were performed for 2 h until complete dissolution of the powder was achieved. The solution was then diluted with 1000 mL of deionized water. The total amount of K and Mn in the powder was first determined by atomic absorption spectroscopy (AAS). Then the Mn^{4+} was determined from As_2O_3 titration.[23] Mn^{3+} is obtained by the difference between the total Mn amount and Mn^{4+}. The total K^+ content and the corresponding Mn^{3+} amount are assumed to be present as MnOOK. The remaining Mn^{3+} ions are assigned to MnOOH, which gives the amount of hydrogen atoms y in $K_xMn^{4+}_{(1-x-y)}Mn^{3+}_{(x+y)}O_2H_y \cdot mH_2O$. The extra weight that remains after accounting for MnO_2, MnOOK, and MnOOH has been ascribed to physisorbed and chemisorbed (or structural) water. According to this, the resulting formula of our material is $K_{0.05}MnO_2H_{0.10} \cdot 0.15H_2O$.

Preparation of the Electrodes. Unless otherwise specified, the electrodes were prepared by mixing 80 wt % of MnO_2 powder with 7.5 wt % of acetylene black (Alfa Aesar, >99.9%, S. A. 80 m^2/g), 7.5 wt % of graphite (Alfa Aesar, conducting grade, −200 mesh), and 5 wt % of poly(tetrafluoroethylene) dried powder (PTFE). The three first constituents were first mixed together in an agate mortar until a homogeneous black powder is obtained. PTFE was then added with a few drops of ethanol. This resulted in a rubber-like paste that was rolled in a film (100−200-μm thick) on a flat glass surface and dried 1 h under vacuum at room temperature. Pieces of the film (0.25 cm^2) were cut and pressed at 9 t/cm^2 on stainless steel grids (AISI 304), which were used as current collectors.

Characterization of the Materials and Electrodes. The crystallographic structure of the powder was investigated using a Siemens D-5000 X-ray diffractometer (Co Kα radiation, 0.1788965 nm) in a $\theta/2\theta$ geometry. The microstructure of the samples was observed with a Leica Stereoscan 440 scanning electron microscope (SEM) coupled with an energy-dispersive X-ray (EDX) analyzer (Oxford Instrument) for the semiquantitative analysis. Single-point Brunauer−Emmett−Teller (BET) surface area measurements were made with a Micromeritic surface area analyzer using N_2 gas.

XPS measurements were performed with a VG Escalab 220i-XL system equipped with a hemispherical analyzer and an aluminum anode. Curve fitting of the XPS data was carried out with the Origin software (version 6.0). The binding energies were corrected for surface charging by referencing to the designated hydrocarbon C 1s binding energy as 284.5 eV.

Electrochemical tests were performed with a EG & G Princeton Applied Research potentiostat M263A operated under Corrware II software (Scribner Associates). A Hg/Hg_2SO_4 (saturated K_2SO_4) assembly and a platinum gauze were used as the reference and counter electrode, respectively, for neutral and acidic electrolytes. A Hg/HgO in 7 M KOH was used as the reference electrode with 1 M NaOH electrolyte. The different electrolytes tested will be specified when needed. Specific capacitance was calculated by integrating either the oxidative or the reductive part of the cyclic voltammogram over the potential window of the CV. All the specific capacitances are reported per gram of active material α-MnO_2 unless otherwise specified. It must be noted that due to the method used for the preparation of the electrodes, an uncertainty of ±10% must be evaluated for all the capacitance values of capacitance reported in this manuscript.

Results and Discussion

Structural and Microstructural Analysis. Figure 1 shows the X-ray diffraction (XRD) patterns of the MnO_2 powder as-synthesized (Figure 1a) and annealed at 300 °C (Figure 1b), 450 °C (Figure 1c), and 600 °C (Figure 1d) for 3 h. The as-synthesized powder is poorly crystallized and the XRD pattern is characterized by broad peaks. The main peaks of the α-MnO_2 cryptomelane[24] can be roughly identified. However, the splitting of each reflection in two or more broad peaks suggests that the MnO_2 powder is a mixture of poorly crystallized microdomains with slightly different cell parameters. This can be due to a variation of the potassium content in each domain, which can vary since there is a lack of potassium (K/Mn atomic ratio = 0.05) compared to the standard cryptomelane phase $K_{2-x}Mn_8O_{16}$. The crystallite size estimated according to the Scherrer equation[25] is in the range 10−20 nm.

Upon subsequent annealing at 300 °C, the crystallite size increased up to 30 nm and a rearrangement of the structure occurred. The average cell parameters for this compound, $a = b \approx 0.98(2)$ nm, $c \approx 0.28(6)$ nm, are consistent with those expected for α-MnO_2 cryptomelane ($I4/m$ space group, $a = b = 0.9815$ nm, $c = 0.2847$ nm [24]).

(19) See for example: Patrice, R.; Gérand, B.; Leriche, J. B.; Seguin, L.; Wang, E.; Moses, R.; Brandt, K.; Tarascon, J. M. *J. Electrochem. Soc.* **2001**, *148*, A448.

(20) Bach, S.; Pereira-Ramos, J. P.; Baffier, N. *Solid State Ionics* **1995**, *80*, 151.

(21) Gaines, R. V.; Skinner, H. C. W.; Foord, E. E.; Masson, B.; Rosenzweig, A. *Dana's New Mineralogy*: *The System of Mineralogy of James Dwight Dana and Edward Salisbury Dana*, 8th ed.; Wiley: New York, 1997.

(22) See for example: Parida, K. M.; Kanungo, S. B.; Sant, B. B. *Electrochim. Acta* **1981**, *26*, 435; Hirano, S.; Narita, R.; Naka, S. *Mater. Res. Bull.* **1984**, *19*, 1229. Dai, J.; Li, S. F. Y.; Siow, K. S.; Gao, Z. *Electrochim. Acta* **2000**, *45*, 2211.

(23) Vogel, A. I. *Quantitative Inorganic Analysis including Elementary Instrumental Analysis*, 3rd ed.; Longman: Essex, U.K., 1962; p 296.

(24) Kondrashev; Zaslavskij *Izv. Akad. Nkad. SSSR, Ser. Fiz.* **1951**, *15*, 179.

(25) Guinier, A. *Théorie et Pratique de la Radiocristallographie*; Guinier, A., Ed.; Dunod: Paris, 1964.

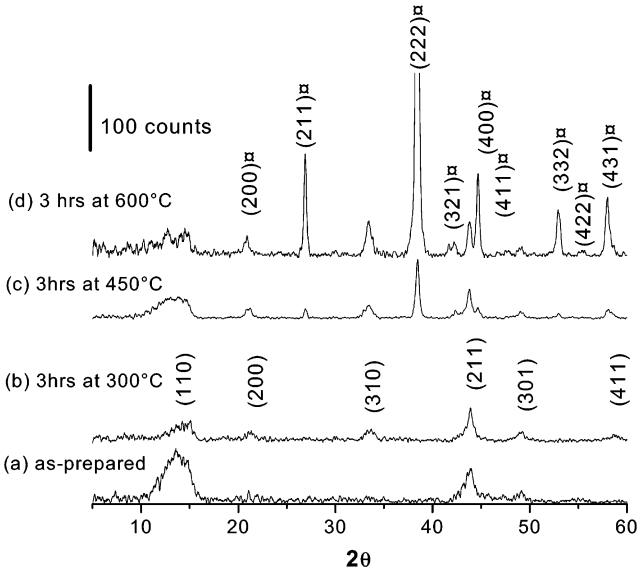

Figure 1. XRD patterns of MnO_2 powder (a) as-prepared and after thermal treatment for (b) 3 h at 300 °C, (c) 3 h at 450 °C, and (d) 3 h at 600 °C. The Co Kα radiation (0.1788965 nm) was used; indexation of cryptomelane α-MnO_2 is given as (*hkl*); indexation of bixbyte-C is given as (*hkl*)○; all the patterns are normalized to the intensity of (211) reflection of cryptomelane (theoretically most intense peak of the cryptomelane XRD pattern).

However, the asymmetric shape of (110), (211), and (411) reflections indicates a high level of stacking faults in the sample. When the temperature is raised above 400 °C, a decomposition of α-MnO_2 in α-Mn_2O_3 (bixbyte-C, *Ia*3 space group, $a = 0.94091$ nm[26]) is observed, and at 600 °C, the well-crystallized bixbyte-C becomes the main phase in the powder.

The microstructure of the as-synthesized α-MnO_2 powder can be observed in Figure 2. The powder is a mixture of platelets such as grains 100-nm wide and 20-nm thick. Thus, the crystallite size determined from these photomicrographs is 5−10 times larger than those deduced from the XRD patterns (10−20 nm). This suggests that each grain observed by SEM is made of several poorly crystallized domains disoriented one from another.

A rough calculation of the specific surface estimated using the geometric surface of platelets such as grains (100-nm diameter, 20-nm thick) indicates a value close to 30 m^2/g. The effective specific surface determined from BET measurements, 180 ± 30 m^2/g, is larger than this value, thus indicating that pores and voids exist inside the grain examined by SEM photomicrographs. Specific surface areas as high as 300 m^2/g have also been reported for α-MnO_2 prepared by similar synthetic procedures.[14,16] It is noteworthy to point out that such a simple coprecipitation method leads to α-MnO_2 powder with relatively high surface area.

Chemical Analysis. The K/Mn atomic ratio determined by EDX analysis (0.050) is in very good agreement with that determined by AAS (0.047). According to the chemical formula of our compound, $K_{0.05}MnO_2H_{0.10}\cdot 0.15H_2O$, the average oxidation state of manganese in this material is 3.85 (see Supporting Information, Table 1).

The manganese average oxidation state was also estimated from the multiplet splitting of the Mn 3s core level spectrum (Figure 3), also referred to as exchange or electrostatic splitting, determined from the XPS analysis.[27−29] The splitting of the 3s peak increases when the valence of Mn in the oxide decreases due to fewer unpaired electrons in the 3d level (see Supporting Information). A graphical representation of the separation of peak energies (ΔE) as a function of the manganese oxidation state from the literature data[27,30] is given in Figure 4. For the as-prepared α-MnO_2 powder, the energy splitting of Mn 3s is 4.83 eV. This value is slightly higher than those reported for β-MnO_2 and is consistent with the presence of Mn(III) in our compound. (β-MnO_2 pyrolusite does not contain additional cations, which will introduce Mn(III) into the structure.) According to the value of ΔE, Figure 4 indicates an average oxidation state of manganese close to 3.8, which is in good agreement with that estimated from chemical analysis. Additionally, the separation of peak positions between the Mn $2p_{3/2}$ and the O 1s component at the lowest position (Mn−O value of 112.5 eV) is consistent with a high Mn(IV) content in our material (see Supporting Information, Table 2).[27]

Electrochemical Analysis, Effect of Electrolyte. Figure 5a shows the cyclic voltammogram for the α-MnO_2 composite electrode in aqueous 0.1 M Na_2SO_4 electrolyte within a potential window range of −0.8 to +0.9 V vs Hg/Hg_2SO_4. For a potential more negative than −0.4 V, a faradaic process is observed and might correspond to the reduction of α-MnO_2. An irreversible anodic wave is detected for a potential more positive than 0.5 V, at about 0.65 V. The onset of solvent oxidation is also observed at the positive potential limit. Similar cyclic voltammetry behavior was recently reported for amorphous hydrous manganese oxide in the same electrolyte.[17] Therefore, it seems useful to limit the potential window for the cyclic voltammetry experiment to −0.4/+0.5 V vs Hg/Hg_2SO_4 when α-MnO_2 is used in the 0.1 M Na_2SO_4 electrolyte. Within this potential range, the shape of the cyclic voltammogram (Figure 6) is roughly a rectangular mirror image characteristic of capacitive behavior and in agreement with literature data.[14−18] An average specific capacitance of 166 F/g can be computed from the data of Figure 6 (see Experimental Section).

A different shape of cyclic voltammogram is observed in acidic media (0.3 M H_2SO_4, Figure 5b). It does not correspond to pseudocapacitive behavior as irreversible anodic and cathodic redox processes are occurring in this medium. A dissolution of MnO_2 is noticed and this electrolyte cannot be used for electrochemical supercapacitor application.[17] In an alkaline electrolyte (1 M NaOH, Figure 5d) the cyclic voltammogram is characterized by irreversible redox processes at about −0.2, 0.6, 0.9, and above 1 V. The first three can be associated with redox transitions of manganese oxides (hydroxides)

(26) Geller, S. *Acta Crystallogr. Sect. B* **1971**, *27*, 821.
(27) Chigane, M.; Ishikawa, M. *J. Electrochem. Soc.* **2000**, *147*, 2246.
(28) Carver, J. C.; Schweitzer, G. K.; Carlson, T. A. *J. Chem. Phys.* **1972**, *57*, 973.
(29) Briggs, D.; Rivière, J. C. *Practical Surface Analysis*; Briggs, D., Seah, M. P., Eds.; John Wiley & Sons: Chichester, 1990; Vol. 1, p 128.
(30) Oku, M.; Hirokawa, K.; Ikeda, S. *J. Electron. Spectrosc. Relat. Phenom.* **1975**, *7*, 465.

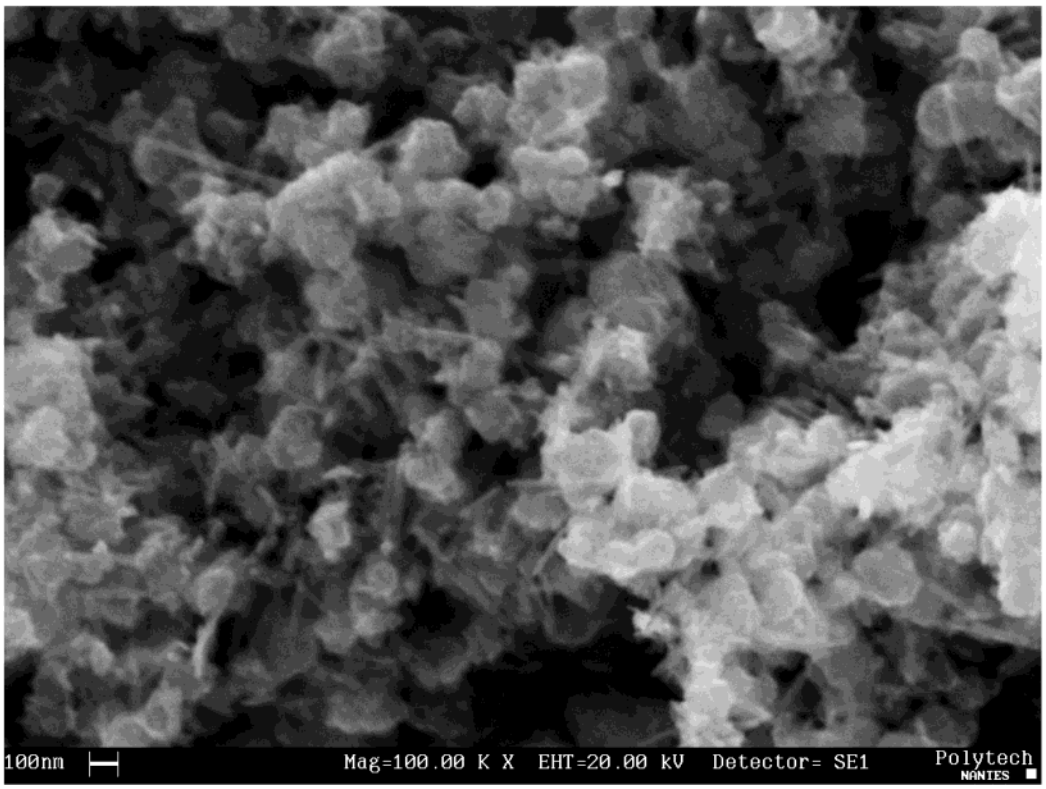

Figure 2. SEM top view of MnO_2 powder (as-prepared); white bar on the left-hand corner is 100 nm.

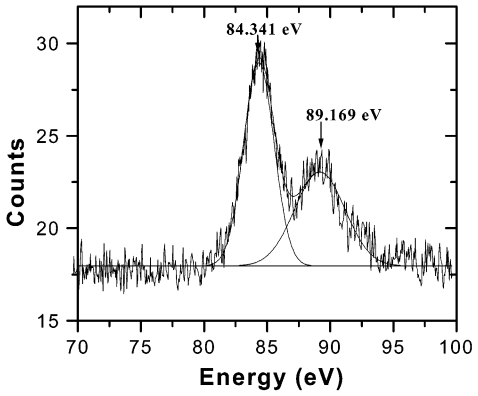

Figure 3. Deconvolution of XPS multiplet splitting Mn 3s with two components. The ΔE value is related to the average oxidation state of manganese.

between different valence states of manganese and the last one is related to the onset of oxygen evolution.[31] Although MnO_2 could be used in alkaline batteries, it is clear that its nonreversible electrochemical behavior in alkaline media prevents its use in electrochemical capacitors. The 0.5 M K_2HPO_4/KH_2PO_4 buffer solution is apparently more favorable than Na_2SO_4 to obtain good capacity within the potential range −0.4/+0.5 V. However, the shape of the cyclic voltammogram indicates that the pseudocapacitive behavior of the α-MnO_2 electrode is strongly limited in this electrolyte, and significant polarization is observed. According to these results, 0.1 M Na_2SO_4 was chosen as the electrolyte for further testing of α-MnO_2. It is interesting to use such a mild, environmentally friendly solution for the development of α-MnO_2-based electrochemical capacitors.

(31) Ratieuville, Y.; Wu, W. L.; Lincot, D.; Vedel, J.; Yu, L. T. *J. Electrochem. Soc.* **1999**, *146*, 3161.

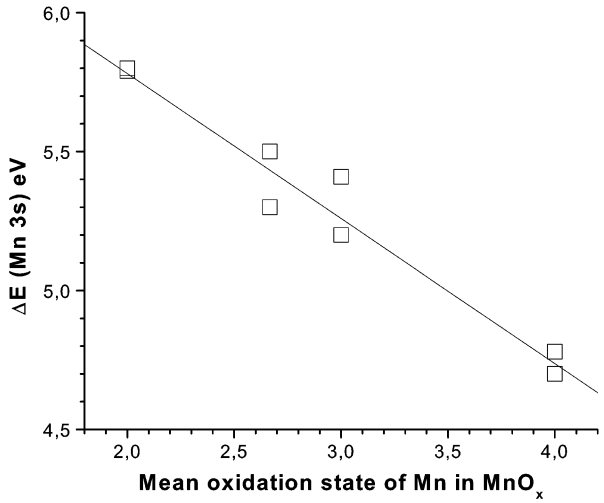

Figure 4. Separation of peak energies ΔE representative of the Mn 3s multiplet splitting as a function of the mean manganese oxidation state according to sample data from refs 27 and 30.

Effect of Scan Rate. Figure 6 illustrates the effect of scan rate on the cyclic voltammetry behavior of the MnO_2 electrode in the 0.1 M Na_2SO_4 electrolyte. The response of the electrode differs from that expected for ideal pseudocapacitive behavior for a sweep rate higher than 5 mV/s due to some polarization. This means that charge (or discharge) of the α-MnO_2 electrode cannot be fully achieved at this time scale (e.g., charge/discharge in about 2 min). However, this time scale represents an appropriate time regime that can allow the use of MnO_2-based electrochemical supercapacitors in many applications where standard rechargeable batteries will be otherwise damaged. This behavior is less favorable than that of α-MnO_2 thin films studied

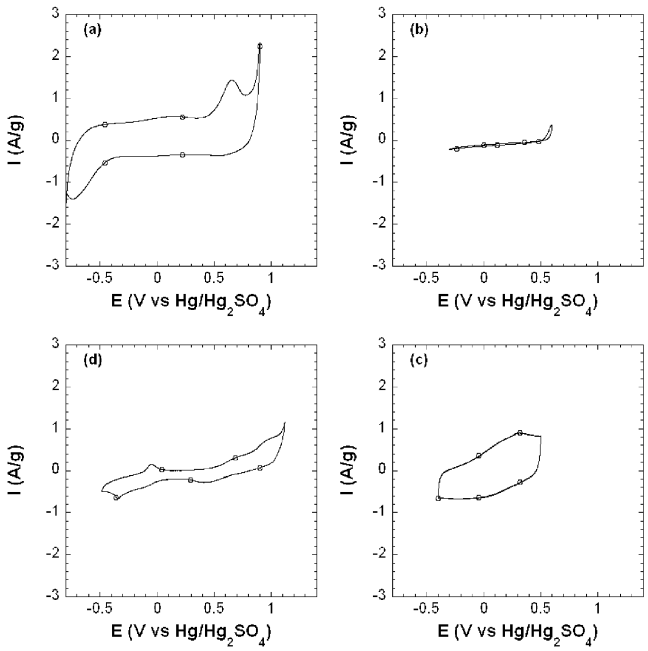

Figure 5. Cyclic voltamogram of α-MnO_2 electrode at a scan rate of 2 mV/s in different aqueous electrolytes: (a) 0.1 M Na_2SO_4; (b) 0.3 M H_2SO_4; (c) 0.5 M K_2HPO_4/KH_2PO_4; (d) 1 M NaOH.

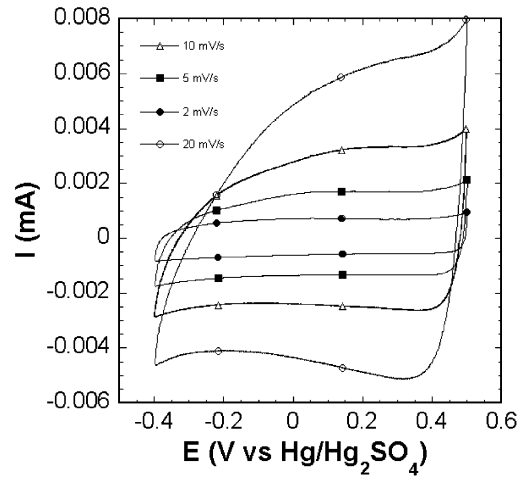

Figure 6. Effect of scan rate on the yclic voltamogram of α-MnO_2 electrode in aqueous 0.1 M Na_2SO_4.

by Anderson and co-workers,[15,18] which can be cycled at a sweep rate as high as 50 mV/s. However, it is comparable with other studies using MnO_2 composite electrodes.[14,16,17] The limitation observed in the case of a "bulk" composite α-MnO_2 electrode highlights the importance of the ionic diffusion throughout the electrode. However, a decrease of the composite electrode thickness from 200 to 100 μm does not induce a change in the specific capacitance either in the response at different sweep rates.

The voltammetric charges have been determined as a function of the sweep rate (Figure 7). As observed with conducting oxide electrocatalysts prepared by thermal decomposition,[32,33] the voltammetric charge q^* decreases as the potential scan rate (v) is increased. In the case of reversible redox transition, the dependence of q^* on v can be explained by the slow diffusion of charge-compensating ions into pores and cracks of the compound. At high sweep rate, diffusion limitation slows the accessibility of sodium ions and protons to the inner surface of the material, where the diffusion is not hampered. The extrapolation of q^* to $v = \infty$ from the q^* vs $v^{-1/2}$ plot (Figure 7a) gives the outer charge q_0^*. which is the charge on the most accessible active surface.[34] The extrapolation of q^* to $v = 0$ from the $1/q^*$ vs $v^{1/2}$ plot (Figure 7b) gives the total charge q_T^*, that is, the charge related to the whole active surface.[34]

At very low sweep rate, q_T^* is determined to be equal to 181 C/g. Although some double-layer charging can significantly contribute to the measured capacitance due to the high surface area of our material, it cannot solely explain the whole capacitance of the electrode. The calculation of the pure double-layer capacitance using the BET surface area (180 m^2/g) by using an average value[1] of 20 $\mu F/cm^2$ gives a specific capacitance of 36 F/g, which is 6 times lower than that measured in this study (166 F/g). Subsequently, it is believed that the main part of the capacitance comes from the pseudocapacitive surface redox process.

If all the Mn cations in $K_{0.05}MnO_2H_{0.10}\cdot 0.15H_2O$ were involved in a faradaic process, the theoretical capacity should be 1051 C/g, that is, nearly six times higher than the limit found at a low sweep rate. This means that the MnO_2 electrode in 0.1 M Na_2SO_4 electrolyte behaves differently than that in an MnO_2-based alkaline battery, where one electron is involved in the first discharge plateau corresponding to the reduction of MnO_2 to amorphous MnOOH in the solid state.[37] However, it must be kept in mind that alkaline cells use strong alkaline media such as 9 M KOH. In alkaline media (1 M NaOH), faradic reactions are also observed for the MnO_2 electrode, which does not act as a pure capacitor (Figure 5d). Consequently, this electrolyte was not selected to study the charge storage properties of the MnO_2 compound.

It will be interesting in the future to understand in which mechanism are involved the 0.17 electrons corresponding to the capacity of the MnO_2 electrode in 0.1 M Na_2SO_4 electrolyte. In fact, 181 C/g corresponds to 1.006 C/m^2 using the BET surface area determined for our material (180 m^2/g). This value suggests that a maximum of 6.3×10^{14} Mn atoms/cm^2 should be involved in the pseudocapacitive behavior of α-MnO_2 synthesized in this study. This value is consistent with the estimated number of Mn atoms per surface unit for α-MnO_2 ($\approx 4.2 \times 10^{14}$ Mn atoms/cm^2) calculated from a mean value of Mn atoms in different diffracting planes.[35] Accordingly, this demonstrates that the redox reactions do not seem to take place within the "bulk" of the material, as is the case for RuO_2 electrodes.[1] This suggests that the microstructure rather than the crystallographic structure of our cryptomelane α-MnO_2 compound determines the capacitance and that the

(32) Ardizzone, S.; Fregonara, G.; Trasatti, S. *Electrochim. Acta* **1990**, *35*, 263.
(33) DePauli, C. P.; Trasatti, S. *J. Electroanal. Chem.* **1995**, *396*, 161.
(34) Soudan, P.; Gaudet, J.; Guay, D.; Bélanger, D.; Schulz, R. *Chem. Mater.* **2002**, *14*, 1210.
(35) A calculation of the Mn surface atom density from the α-MnO_2 structure gives $\approx 8.5 \times 10^{14}$ Mn atoms/cm^2 for plane (310), $\approx 6.8 \times 10^{14}$ Mn atoms/cm^2 for plane (211), and no Mn atoms from planes (110) and (200).
(36) Ruetschi, P.; Giovanoli, R. *J. Electrochem. Soc.* **1988**, *135*, 2663.
(37) See for example: Kozawa, A.; Powers, R. A. *J. Electrochem. Soc.* **1966**, *113*, 870.

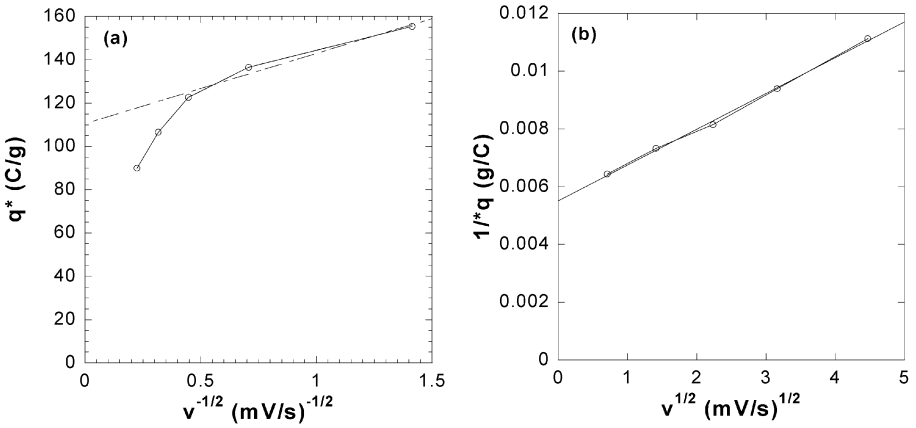

Figure 7. Variation of the voltametric charge (q^*) with respect to the sweep rates v: (a) extrapolation of q^* to $v = \infty$ from the q^* vs the $1/v^{1/2}$ plot gives the outer charge q_0^* (charge on the most accessible active surface); (b) extrapolation of q^* to $v = 0$ from the $1/q^*$ vs $v^{1/2}$ plot gives the total charge q_T^*(charge related to the whole active surface).

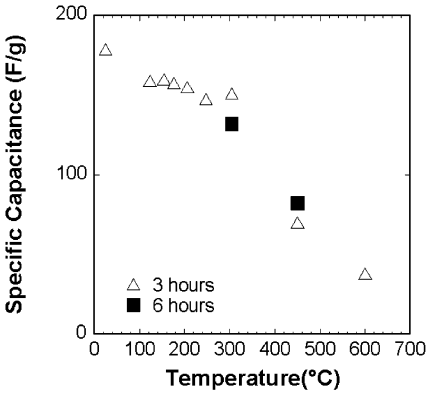

Figure 8. Effect of heat treatment on the specific capacitance of α-MnO_2 electrodes determined from cyclic voltammetry at a sweep rate of 2 mV/s in 0.1 M Na_2SO_4 within a potential window of −0.4 to +0.5 V vs Hg/Hg_2SO_4.

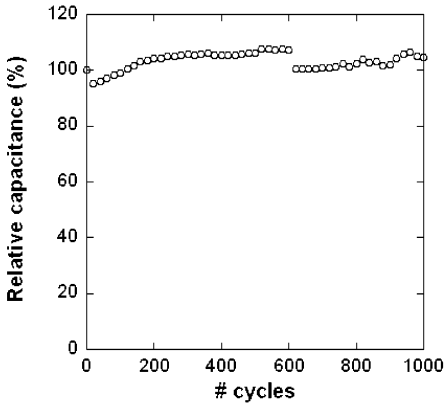

Figure 9. Variation of the specific capacitance as a function of the number of cycles. The potential cycling was performed in 0.1 M Na_2SO_4 within a potential window ranging from −0.4 to +0.5 V vs Hg/Hg_2SO_4 at a sweep rate of 2 mV/s.

intercalation of Na^+ ions and/or protons in the 2 × 2 tunnels of the cryptomelane structure do not seem to be much involved in the redox processes or that "intercalation" occurs within a very limited thickness. Practically, this implies that the specific capacitance of our α-MnO_2 powder is strictly limited by the BET surface area of the powder and by its molecular weight, that is, its chemical composition. An increase in the surface area will enhance the specific capacitance of our material. A decrease in the molecular weight will lead to the same effect. A simple calculation shows that, for $K_{0.05}MnO_2H_{0.10}\cdot 0.15\ H_2O$, the total loss of H_2O by annealing would only lead to a decrease of 3% of its molecular weight and subsequently only a small gain on the specific capacitance.

At high sweep rate, the outer charge reached a limit of 110 C/g, indicating that only half of the manganese surface atoms participate in the faradaic process. One explanation can be that such a high rate limits the diffusion of Na^+ ions and/or protons throughout the whole volume of the MnO_2 electrode and consequently some pores and voids remain inaccessible at high sweep rates.

Effect of Annealing Temperature on Capacitance. In Figure 8, the specific capacitances, measured on a cyclic voltammogram at a rate of 2 mV/s, is plotted as a function of the annealing temperature for two different annealing times. The as-precipitated powder shows the highest specific capacitance (180 F/g). Following a decrease of the capacitance to about 160 F/g (loss of 12%) after heating for 3 h between 100 and 200 °C, a monotonic decrease is observed between 200 and 600 °C. Three hours of annealing time at 600 °C induces a capacitance of only 40 F/g, that is, 22% of the initial capacitance. The heat treatment at a temperature between 100 and 200 °C is believed to remove both physically and chemically adsorbed water molecules[15,36] and decrease the surface area of the active material. The loss of water molecules should lead to a small increase of the capacitance[15] whereas the surface area decrease should induce a decrease of the capacitance. The data of Figure 8 clearly show that the latter has the most significant effect. Above 400 °C, the decomposition of α-MnO_2 into Mn_2O_3, as shown on the XRD patterns (Figure 1c,d), leads to a drastic fade of the specific capacitance.

Long-Term Stability upon Cycling. The long-term stability of composite electrodes based on as-prepared powder upon cycling was investigated and the variation of specific capacitance over 1000 cycles is depicted in Figure 9. A 6% loss of capacitance is observed during the first 20 cycles and thereafter the capacitance increases up to 105% of its initial value. Such an improvement of the specific capacitance upon cycling has already been reported for MnO_2 thin films.[15] After 200 cycles, the capacitance remains stable and close to 105% of the starting value. After 600 cycles, the electrode was

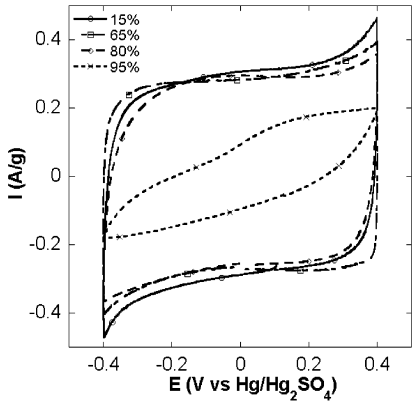

Figure 10. Cyclic voltammogram of different α-MnO_2 composite electrodes in 0.1 M Na_2SO_4 at a sweep rate of 2 mV/s: (a) 95% MnO_2, (b) 80% MnO_2, (c) 65% MnO_2, and (d) 15% MnO_2. The composite electrode also contains 5% of PTFE and the remainder is made of equal quantities of graphite and carbon black (see Supporting Information, Table 3).

stopped and another batch of 400 cycles was recorded. Despite the small drop of the capacitance after the 600th cycle and the beginning of the last 400 cycles, the capacitance of the electrode is identical to that of the first cycle. The electrode can withstand 1000 cycles without significant capacitance loss. This demonstrates that, within the voltage window −0.4/+0.5 V vs Hg/Hg_2SO_4, the charge and discharge processes do not seem to induce significant structural or microstructural changes of the electrode as expected for pseudocapacitive reactions. This long-term stability is also in good agreement with a surface mechanism rather than with bulk reactions, which will have inevitably resulted in the degradation of the structure of the electrode and subsequently should have induced a capacitance fade upon cycling.

Electrode Composition. The electrode composition was also investigated to check if the specific capacitance was limited by the electronic conductivity of the composite electrode (see Supporting Information, Table 3). The amount of binder was kept constant while varying the amount of α-MnO_2 and conductive additive (graphite and acetylene black). In these experiments (Figure 10), the potential window has been limited to −0.4/+0.4 V vs Hg/Hg_2SO_4. The sample with no conductive additive (95% MnO_2, 5% PTFE) does not show ideal capacitive behavior. The poor intrinsic electronic conductivity of α-MnO_2 provides high polarization of the electrode. In contrast, a satisfying rectangular cyclic voltammogram is recorded when at least 15% of conductive carbon is added. If the capacitance values are reported per gram of MnO_2, the highest value is reached with a high carbon content (80%), although a lower carbon content of 15% yielded satisfactorily values. The high capacitance values in the presence of a high carbon content reflect the low conductivity of MnO_2. However, a high amount of carbon leads to very poor capacitance when reported per gram of electrode. Finally, 80% of active material and 15% of carbon seems to be an optimized composition.

Capacitance of Various MnO_2-Based Electrodes. The significant difference in the capacitance values reported in the literature for MnO_2 deserves some comments. The most common capacitances[14,16,17] vary between 150 and 300 F/g, which is within the range that was obtained in this study. On the other hand, significantly higher values were also recently reported for sol−gel and colloidal tetrapropylammonium manganese oxide materials.[15,18] We believe that the difference stems from the much smaller film thickness used in the latter studies. The thickness of these films was estimated to be in the range of 25 nm, which is several orders of magnitude thinner than those used in other studies[14,16,17] and in the present work. A smaller capacitance reflects a smaller utilization of the active material upon cycling. Nonetheless, the capacitance values in the range of 200 F/g are attractive values for application of these materials in electrochemical supercapacitors due to their low cost and ease of preparation.

Conclusion

A low-cost α-MnO_2 cryptomelane compound synthesized with a very simple coprecipitation technique was tested as possible electrode material for an electrochemical supercapacitor. The chemical composition of the powder has been determined to be $K_{0.05}MnO_2H_{0.10}\cdot 0.15H_2O$. Interesting pseudocapacitance behavior has only been observed in an environmentally friendly electrolyte (0.1 M Na_2SO_4) and an average capacitance as high as 166 F/g was reproducibly obtained within a 0.9-V electrochemical window (voltage range −0.4/+0.5 V vs Hg/Hg_2SO_4) using a sweep rate of 2 mV/s. The data suggest that only the Mn surface atoms are involved in the pseudocapacitive redox processes. Therefore, the high specific capacitance seems to be related to the high surface area of the MnO_2 powder rather than intercalation of Na^+ ions and/or protons in the bulk of α-MnO_2, as is the case for protons insertion in hydrated RuO_2 materials. α-MnO_2 composite electrode (80 wt % of active material) can withstand 1000 cycles with stable capacitance. These results confirm the potential of MnO_2 as a possible active electrode material for an electrochemical supercapacitor and they underline the influence of the microstructure of the material. The effect of the structure and the microstructure will be investigated by testing several MnO_2 compounds with tunnels or layered structures and the results of these studies will be reported elsewhere. In addition, it might be interesting to investigate the influence of doping elements (e.g., bismuth [38]) on the capacitive behavior of MnO_2.

Acknowledgment. The authors would like to thank Dr. Pascal Fragnaud from Laboratoire de Génie des Matériaux, Nantes, for his help with the XRD and BET measurements. Dr. Thierry Brousse would like to thank UQAM for welcoming him as a visiting professor.

Supporting Information Available: Origin of the Mn 3s peak separation in the XPS spectra, table summarizing the chemical analysis on as-prepared α-MnO_2 powder, table of the XPS peak analyses of α-MnO_2 powder and references data from the literature, and table of the electrode composition and specific capacitance of the composite electrodes presented in Figure 10 (PDF). This material is available free of charge via the Internet at http://pubs.acs.org.

CM020408Q

(38) See for example: Wroblowa, H. S.; Gupta, N. *J. Electroanal. Chem.* **1987**, *238*, 98. Kannan, A. M.; Bhavaraju, S.; Prado, F.; Manivel Raja, M.; Manthiram, A. *J. Electrochem. Soc.* **2002**, *149*, A483.